Environmental Science Nano

PAPER

View Article Online
View Journal | View Issue

Cite this: *Environ. Sci.: Nano*, 2018, 5, 1567

Hydroxyl radical scavenging by cerium oxide nanoparticles improves *Arabidopsis* salinity tolerance by enhancing leaf mesophyll potassium retention†

Honghong Wu, [a] Lana Shabala, [b] Sergey Shabala [b] and Juan Pablo Giraldo *[a]

Received 19th March 2018,
Accepted 21st May 2018

DOI: 10.1039/c8en00323h

rsc.li/es-nano

Salinity is a widespread environmental stress that severely limits crop yield worldwide. Cerium oxide nanoparticles (nanoceria) have the unique capability of catalytically reducing levels of stress-induced reactive oxygen species (ROS) including hydroxyl radicals (˙OH) that lack enzymatic scavenging pathways. The underlying mechanisms of how nanoceria ROS scavenging augments plant tolerance to environmental stress are not well understood. Herein, we demonstrate that catalytic ˙OH scavenging by nanoceria in *Arabidopsis thaliana* leaves significantly improves mesophyll K^+ retention, a key trait associated with salinity stress tolerance. Leaves with mesophyll cells interfaced with 50 mg L^{-1} poly(acrylic acid) coated nanoceria (PNC) have significantly higher ($P < 0.05$) carbon assimilation rates (85%), quantum efficiency of photosystem II (9%), and chlorophyll content (14%) compared to controls after being exposed to 100 mM NaCl for 3 days. PNC infiltrated leaves (PNC-leaves) under salinity stress exhibit lower ROS levels – including hydroxyl radical (41%) and its precursor hydrogen peroxide (44%) – and one fold higher ($P < 0.05$) cytosolic K^+ dye intensity in leaf mesophyll cells relative to controls. Non-invasive microelectrode ion flux electrophysiological (MIFE) measurements indicated that PNC-leaves have about three-fold lower NaCl-induced K^+ efflux from leaf mesophyll cells compared to controls upon exposure to salinity stress. The ROS-activated nonselective cation channels (ROS-NSCC) in the plasma membrane of leaf mesophyll cells were identified as the main ˙OH-inducible K^+ efflux channels. Long term catalytic scavenging of ˙OH in leaves by PNC enhances plant photosynthetic performance under salinity stress by enabling plasma membrane channels/transporters to coordinately retain higher levels of K^+ in the leaf mesophyll cell cytosol. PNC augmented plant ROS scavenging provides a key tool for understanding and improving plant tolerance against abiotic stresses such as salinity.

Environmental significance

Environmental stresses, including salinity, lead to the accumulation of reactive oxygen species (ROS) with subsequent damage to plant cellular components, reduced crop growth and yield. Organisms lack enzymatic pathways for catalytically scavenging hydroxyl radicals, one of the most destructive ROS, thus limiting the ability of molecular tools to manipulate this ROS *in vivo*. Herein, we apply a nanobiotechnology-based approach that improves plant salinity stress tolerance by scavenging hydroxyl radicals and its precursors. We determined the underlying mechanisms of how cerium oxide nanoparticle (nanoceria) reduction of hydroxyl radical levels in *Arabidopsis* leaves affects potassium fluxes across the plasma membrane. Nanoceria enable higher retention of K^+ in leaf mesophyll, thus improving plant photosynthetic performance and biomass against environmental stress *e.g.* salinity.

1. Introduction

Salinity is a global issue threatening agricultural production in more than 50% irrigated land worldwide.[1,2] Salt stress perturbs the equilibrium between reactive oxygen species (ROS) production and scavenging resulting in ROS accumulation with subsequent damage to proteins, lipids, carbohydrates, and DNA.[3,4] Among several ROS – hydrogen peroxide, superoxide anion, hydroxyl radicals and singlet oxygen – hydroxyl radicals are the most destructive ROS and cannot be scavenged by any known enzymes in biological systems.[3,5] Hydroxyl radicals (˙OH) have an extreme reactivity and a very short lifetime (~1 ns).[6] These radicals are mainly generated in chloroplasts and mitochondria in plants under stress

[a] *Department of Botany and Plant Sciences, University of California, Riverside, California 92521, USA. E-mail: juanpablo.giraldo@ucr.edu; Tel: +1 9518273583*
[b] *School of Land and Food, University of Tasmania, Hobart, Tasmania 7001, Australia*

† Electronic supplementary information (ESI) available. See DOI: 10.1039/c8en00323h

condition.[3,4] They are produced by the Fenton reaction biosynthesis pathway; a series of reactions that require H_2O_2 and transition metals as precursors.[3,7] Genetic engineering approaches are not currently applicable for counteracting the damage directly caused by $^{\bullet}OH$ in plants under abiotic stress. To the best of our knowledge, there are no reported methods to catalytically reduce $^{\bullet}OH$ *in planta*.

Nanomaterials have distinct chemical, optical, and mechanical properties that can be applied as tools to study and engineer biological mechanisms in wild-type plants.[8–12] Cerium oxide nanoparticles (nanoceria) are potent catalytic scavengers of ROS including $^{\bullet}OH$, hydrogen peroxide (H_2O_2), and superoxide anion.[13,14] Nanoceria have a large number of surface oxygen vacancies that alternate between two oxidation states (Ce^{3+} and Ce^{4+}).[15–17] The Ce^{3+} dangling bonds effectively scavenge ROS while the lattice strains at the nanoscale promote the regeneration of these defect sites *via* redox cycling reactions.[18] Giraldo *et al.*[8] showed that nanoceria (24 μM) catalytically scavenges both superoxide anion and hydrogen peroxide in isolated chloroplasts. Wu *et al.*[19] reported that anionic nanoceria coated with poly(acrylic acid) (PNC, 51 mg L^{-1}) having low Ce^{3+}/Ce^{4+} ratios significantly reduce ROS accumulation and improve photosynthetic performance in plants under abiotic stresses. Negatively charged nanoceria are more efficiently delivered to chloroplasts than their positively charged counterparts. Furthermore, low Ce^{3+}/Ce^{4+} (~35%) nanoceria have catalase (CAT) and super oxide dismutase (SOD) mimetic activity in plants.[16,19]

The study of plant–nanoceria interactions has mainly focused on nanoceria uptake and distribution,[20–24] and the effect of nanoceria on antioxidant enzyme activities,[25,26] photosynthetic performance,[27,28] and abiotic stress tolerance.[19,29] Recently, we reported that negatively charged nanoceria (10 ± 1.3 nm, ~50 mg L^{-1}) augment ROS scavenging and photosynthetic performance of *Arabidopsis* plants under high light, heat, and dark chilling.[19] Similarly, previous studies have shown that anionic nanoceria enhance photosynthetic rates in soybean (100 mg kg^{-1}) (*Glycine max* L. Merr.)[28] and increase shoot biomass in carrot (50 mg kg^{-1}) (*Daucus carota* cv. Danvers Half Long).[20] Negatively charged nanoceria (200–1000 mg kg^{-1}) applied to soil also improve net photosynthetic rates and leaf biomass in canola (*Brassica napus* cv. Dwarf Essex) exposed to salt stress (100 mM NaCl).[27] The underlying mechanisms of how nanoceria ROS scavenging improves plant tolerance to environmental stress such as salinity are not well understood. It has been shown that mesophyll K^+ retention is a key trait conferring plant salt tolerance,[30–32] mainly controlled by K^+ efflux from the cytosol to the apoplast. The plasma membrane K^+-selective (GORK) and non-selective (NSCC) cation efflux channels mediate K^+ retention in plants under salt stress.[33] Hydroxyl radicals are known to activate GORK in *Arabidopsis* roots[34] and ROS-activated NSCC channels.[35,36] How hydroxyl radicals affect leaf mesophyll K^+ retention under salinity stress is unclear. Herein, we study the mechanisms of how anionic nanoceria (PNC) *in vivo* scavenging of $^{\bullet}OH$ in leaves impacts plant performance under salinity stress.

Using a plant nanobiotechnology approach we enabled wild-type *Arabidopsis* plants with augmented scavenging of ROS including $^{\bullet}OH$ by embedding PNC in leaf mesophyll tissues. We hypothesized that catalytic $^{\bullet}OH$ scavenging by PNC modulates the activities of K^+ efflux channels and reduces NaCl-induced K^+ efflux from leaf mesophyll cells improving salinity stress tolerance. To assess plant performance under salt stress, we measured chlorophyll content index, shoot biomass, and key light and carbon reaction of photosynthesis parameters. We also quantified PNC ability for *in vivo* scavenging of $^{\bullet}OH$ and its impact on mesophyll K^+ retention. To elucidate the mechanisms of PNC action on mesophyll K^+ retention, we measured changes in leaf plasma membrane K^+ channel activity and gene expression.

2. Materials and methods

2.1. Plant material

Four weeks old *Arabidopsis thaliana* (Columbia 0) plants were grown in pots (2 × 2 inch, 32 inserts) filled with standard soil mix (Sunshine, LC1 mix). After one week germination one individual seedling was kept in each pot. Plants were grown in Adaptis 1000 growth chamber (Conviron) at 200 μmol m^{-2} s^{-1} photosynthetic active radiation (PAR), 24 ± 1 °C and 21 ± 1 °C at day- and night-time, respectively. Relative humidity was maintained at 60%, and day/night regime was 14 h/10 h. Plants were hand-watered with deionized water once every two days.

2.2. Synthesis and characterization of PNC

Low Ce^{3+}/Ce^{4+} ratio cerium oxide nanoparticles (nanoceria) coated with poly(acrylic acid) (PNC) were synthesized and characterized as described in Wu *et al.*[19] Briefly, 1.08 g cerium(III) nitrate (Sigma Aldrich, 99%) and 4.5 g poly(acrylic acid) (1800 MW, Sigma Aldrich) were dissolved in 2.5 mL and 5.0 mL molecular biology grade water (Corning, Mediatech, Inc.), respectively. The solutions were mixed thoroughly at 2000 rpm for 15 min using a vortex mixer and added dropwise to a 50 mL beaker containing 15 mL, 30% ammonium hydroxide solution (Sigma Aldrich). The mixture was stirred at 500 rpm for 24 h at ambient temperature, then centrifuged at 4000 rpm for 1 h to remove any debris and large agglomerates. The supernatant was purified from free polymers and other reagents by centrifugation at 4500 rpm (Allegra X30, Beckman) using a 10 K Amicon cell (MWCO 10 K, Millipore Inc.) for at least six cycles (15 min each cycle). After each cycle, the eluent absorption spectrum was measured in a UV-VIS spectrophotometer (UV-2600, Shimadzu) until no peaks of free polymers and other reagents were detected. The purified PNC suspension was filtered through a 20 nm pore size syringe filter (Whatman, Anotop™ 25). The final PNC solution was stored in a refrigerator (4 °C) until further use.

The concentration of the final PNC solution was calculated from the absorption spectrum measured by the UV-VIS spectrophotometer (UV-2600, Shimadzu) (Fig. S1A†) using

Beer–Lambert's law ($A = \varepsilon CL$) with absorbance at 271 nm, absorption molar coefficient (ε) of 3 cm^{-1} mM^{-1},[37] and pathway length (L) of 1 cm. C is the molar concentration of the measured sample. Sample concentration in mg L^{-1} was calculated by using the molecular weight of cerium(III) oxide and cerium(IV) oxide weighted by the Ce^{3+}/Ce^{4+} ratios for PNC. Pulido-Reyes *et al.*[16] showed that negligible amounts of dissolved Ce (ranging from 0.00001 to 0.0008 mg l^{-1}) in different types of nanoceria (10 mg L^{-1}). No dissolved $Ce(NO_3)_3$ absorption peaks were found in purified PNC solution.[19] Molecular grade water was used to determine that the resolution of absorbance values collected by the UV-VIS spectrophotometer is less than 0.01.

The hydrodynamic diameter (DLS size) and zeta potential of synthesized PNC are 10 ± 0.6 nm and −17 ± 2.7 mV, respectively. Four separate measurements were conducted. The zeta potential and size of PNC in solution were measured by a Malvern Zetasizer (Nano ZS) (resolution < 0.1 mV) and Sizer (Nano S) (resolution < 0.1 nm, detection limit: 0.3 nm), respectively. Fourier transformed infrared spectroscopy (FTIR) was performed with Nicolet 6700 FTIR (Thermo Electron Corp.) to confirm the presence of –COOH group in PNC (Fig. S1B†). Dried PNC powder were used and the background was collected and subtracted accordingly. The Ce^{3+}/Ce^{4+} ratio measured by XPS is 35 ± 2.2% (Fig. S1C†). Dry samples of PNC were mounted on a carbon tape for XPS (X-ray photoelectron spectroscopy, Kratos Axis Ultra X-ray photoelectron spectroscopy) measurement to characterize the ratio of the Ce^{3+} and Ce^{4+}.

2.3. *In vitro* assay of nanoceria scavenging of hydroxyl radical

The ability of nanoceria to scavenge hydroxyl radicals was tested *in vitro*. Here Cu/Asc (copper/sodium ascorbate) and HPF (hydroxyphenyl fluorescein) dye were used. Cu/Asc mixture generates hydroxyl radicals. HPF remains in non-fluorescent form until it reacts with $^{\bullet}OH$ or peroxynitrite anion. Thus, the hydroxyl radical scavenging ability of PNC can be monitored by measuring the decrease of fluorescence of HPF in the presence of hydroxyl radicals. First, 71.5 μl HPF dye (10 μM, in TES infiltration solution) was transferred into each well (Costar white 96 well microplate with flat bottom, Corning). Then 10 μl ascorbate sodium solution (10 mM, in ddH_2O) and 8.5 μl PNC (5.4 mM, in ddH_2O) added. A solution (10 μl) of copper chloride (3 mM, in ddH_2O) was added into each well and the fluorescence of HPF dye was measured immediately using Victor 2 plate reader (Wallac) at 485/530 nm (excitation/emission) for 15 min. Final PNC concentration in this reaction mixture is 50 mg L^{-1}, the same concentration used *in vivo*. A concentration of 50 mg L^{-1} PNC was previously determined to be optimal for augmenting plant ROS scavenging and enhancing photosynthesis under abiotic stress in *Arabidopsis*.[19] The fluorescence of reaction system without PNC was used as control. To avoid any possible confounding effects, the fluorescence was also measured in HPF alone and also the combination of HPF + $CuCl_2$, HPF + Na-ascorbate and HPF + PNC were tested. The ability of PNC with a low Ce^{3+}/Ce^{4+} ratio to scavenge superoxide anion and hydrogen peroxide was shown previously by Wu *et al.*[19]

2.4. Nanoceria leaf infiltration

Leaves were slowly infiltrated with nanoceria through the leaf abaxial side with ~200 μL of solution (50 mg L^{-1} [19] PNC in 10 mM TES infiltration buffer) by gently pressing the tip of the syringe (NORM-JECT®, 1 ml) against the leaf lamina. A 10 mM TES infiltration buffer solution (10 mM TES, 10 mM $MgCl_2$, pH 7.5) was used as control. Kimwipes were used to gently remove the excess solution remaining on the surface of leaf lamina. Infiltrated plants were kept on the bench under light for leaf adaptation and incubation with nanoceria for 3 h. A detailed protocol for leaf lamina infiltration of nanoparticles is given in Wu *et al.*[38]

2.5. Leaf chlorophyll content

Chlorophyll content index (CCI) was monitored in wild-type *Arabidopsis* plants infiltrated with PNC and buffer solution (controls) for 3 days after onset of the salinity stress (100 mM NaCl). Four week old plants infiltrated with PNC or buffer as explained above were randomly distributed in 1020 greenhouse trays without holes filled with 100 mM NaCl (a commonly used NaCl concentration for *Arabidopsis* salinity stress studies[39–41]). CCI measurements were performed using a chlorophyll meter (SPAD-502 plus, Konica Minolta, Tokyo, Japan; CCI readout resolution: 0.1) with each leaf being measured three times (each time/data point was composed of at least three CCI readout).

2.6. Shoot biomass

Shoot biomass was monitored in PNC- and buffer-infiltrated *Arabidopsis* plants after two weeks of salt stress (100 mM NaCl). Four week old plants infiltrated with PNC or buffer as explained above were randomly distributed in 1020 greenhouse trays without holes filled with 100 mM NaCl. After salt treatment, the above ground plant biomass was collected and weighted immediately. Then, samples were dried in oven at 65 °C for 72 h and dry weight was recorded.

2.7. Leaf gas exchange and chlorophyll fluorescence

Gas exchange and chlorophyll fluorescence measurements were performed in *Arabidopsis* leaves from four week old plants exposed to 3 days of 100 mM NaCl using a GFS-3000 (Walz) as described in Wu *et al.*[19] Leaves larger than the gas analyzer chamber (2.5 × 1 cm^2) and with similar chlorophyll content index were infiltrated with TES infiltration buffer (control) and PNC (50 mg L^{-1} PNC in 10 mM TES infiltration buffer) and incubated for 3 h under room conditions. Leaves were dark adapted for 10 min before Fv/Fm measurements. A-light curve was performed at decreasing light levels from 900, 600, 400, 300, 200, 100, 50 to 0 μmol m^{-2} s^{-1} PAR. The

GFS cuvette temperature was set at 23 °C and 50% relative humidity.

2.8. DAB and NBT staining

DAB (3,3′-diaminobenzidine) and NBT (nitro blue tetrazolium) staining was performed following the protocol by Kumar *et al.*[42] with modifications. DAB (50 mg) and NBT (100 mg) were dissolved in 50 ml ddH_2O (pH adjusted to 3.8 by HCl) and 50 ml sodium phosphate buffer (50 mM, pH 7.5), respectively. Leaves of salt treated plants were excised and placed in 50 ml falcon tubes (wrapped with aluminum foil) with either freshly prepared DAB or NBT solutions and kept overnight at ambient temperature. Then staining solutions were removed and 40 ml of absolute ethanol was added. Samples were placed into a boiling water bath for 15 to 20 min and periodically shaken. Ethanol was removed and leaves placed on a paper towel saturated with 60% glycerol. Pictures were taken with a Nikon Coolpix S7000 camera.

2.9. *In vivo* ROS scavenging by nanoceria

Leaf discs (~5 mm diameter) from the PNC and buffer infiltrated plants (four weeks old) were incubated with either 25 μM 2′,7′-dichlorodihydrofluorescein diacetate (H_2DCFDA, Thermo Fisher Scientific), 10 μM dihydroethidium (DHE, Thermo Fisher Scientific) or 10 μM hydroxyphenyl fluorescein (HPF, Thermo Fisher Scientific) dyes (in TES infiltration buffer, pH 7.5) in 1.5 mL Eppendorf tubes for 30 min under darkness. Incubated samples were mounted on microscope slides inside a well formed by observation gel (Carolina, item 132700) filled with PFD (perfluorodecalin). A coverslip was placed on the top to seal the well ensuring that no air bubbles remain trapped under. The samples were imaged by a Leica SP5 confocal microscope (Leica Microsystems, Germany). Confocal imaging settings were: 40× wet objective; 496 nm laser excitation; line average: 4; PMT1: 500–600 nm; PMT2: 700–800 nm. Three to eight individual assessments (4 leaf discs for each plant) were done. The microscope was manually focused on a region of leaf mesophylls cells. The fluorescence signal from the ROS dyes was collected and recorded. *Z*-Stacks ("*xyz*") of two different regions were taken per leaf disc. *Z*-Stack section thickness of 2 μm; 16 layers per leaf disc. DHE, DCF and HPF fluorescence intensity was measured and analyzed in ImageJ within the imaged region of spongy mesophyll cells using ImageJ software (NIH).

2.10. Live imaging of K^+ distribution in mesophyll cells

Imaging of K^+ distribution in the cytosol and vacuole was performed using 20 μM of the K^+ dye APG-2AM (asante potassium green-2AM, Abcam Biotechnology company) and 20 μM of FM 4-64 (*N*-(3-triethykammoniumpropyl)-4(6-(4-(diethylamino)phenyl)hexatrienyl)pyridinium dibromide, Thermo Fisher Scientific) for plasma membrane and tonoplast staining. The fluorescent dyes were dissolved in pure DMSO and diluted with TES infiltration buffer to working concentration. Leaves of 4 week old *Arabidopsis* plants treated with 100 mM NaCl for 3 days were collected and the epidermis peeled off. Leaf discs were incubated with APG-2 AM and FM-4-64 dyes in 1.5 mL Eppendorf tubes for 2.5 h in darkness. After incubation, leaf discs were rinsed in ddH_20 and mounted on microscope slides for confocal imaging. The confocal imaging settings were: 488 nm laser excitation (30%); PMT1: 520–560 nm; PMT2: 610–630 nm. *Z*-Stacks ("*xyz*") measurement were taken per leaf disc with *Z*-stack section thickness of 2 μm; 16 layers per leaf disc. The layer with strongest fluorescence intensity with APG-2 fluorescence was analyzed by ImageJ software (NIH). The background values were deducted from analysis. Three to five individuals (4 leaf discs for each plant) in total were used for these experiments.

2.11. Mesophyll cell K^+ and H^+ flux measured by MIFE

Net K^+ and H^+ fluxes were measured from leaf segments using non-invasive microelectrode ion flux estimation technique (the MIFE[43,44]). Blank microelectrodes were pulled out from borosilicate glass capillaries (GC 150-10; Harvard Apparatus, Kent, UK) and dried overnight at 225 °C in an oven. The blank microelectrodes were then silanized with tributylchlorosilane (no. 282707, Sigma-Aldrich). After drying and cooling, electrode blanks were back filled with appropriate backfilling solutions (200 mM KCl for K^+, 15 mM NaCl + 40 mM KH_2PO_4, pH adjusted to 6.0 for H^+ microelectrodes). Then the tips of respective microelectrodes were front filled with commercially available selectophore cocktails (cat. no 60031 for K^+ or cat. no 95297 for H^+, Sigma-Aldrich). Microelectrodes were mounted in MIFE electrode holders and calibrated in sets of appropriate standard solutions (see Shabala *et al.*[43] for methodological details). Only microelectrodes with a slope over 50 mV per decade and correlation over 0.999 were used. Leaf segments were cut angularly to expose mesophyll cells and mounted in holders and preconditioned in BSM (basic salt medium; 0.1 mM $CaCl_2$ + 0.5 mM KCl, pH 5.7) solution for 0.5 h. Calibrated microelectrodes were co-focused and aligned with a leaf sample and the electrode tips positioned 40 μm from the exposed mesophyll surface. During measurements, a computer-controlled stepper motor moved electrodes in a 6 s square-wave cycle between two positions, 40 and 110 μm above the exposed mesophyll surface. The recorded electrochemical gradient potential change was converted into net ion flux changes using the calibrated values of the ion selective microelectrodes and cylindrical diffusion geometry of the exposed mesophyll area (MIFEFLUX software[43,44]). At least four leaf segments from different plants were assessed.

2.12. Pharmacological experiments

The identity of K^+ transport systems underlying hydroxyl radicals-induced K^+ efflux from *Arabidopsis* mesophyll cells was investigated in a series of pharmacological experiments using some known ion channel blockers. For K^+ flux experiments, leaf samples of control plants were pre-treated for 1 h with either 20 mM tetraethyl ammonium chloride (TEA^+, a

known blocker of K^+ selective channels[32]) or 0.1 mM gadolinium chloride (Gd^{3+}, a known blocker of NSCC channels[32]). Steady-state K^+ fluxes were recorded over a period of 5 min. Then, Cu/Asc (0.3 mM/1 mM) mixture was administered to the measuring chamber and kinetics of net K^+ fluxes recorded for a further 20 min. All chemicals used were from Sigma-Aldrich.

2.13. Plasma membrane potential measurement

Conventional KCl-filled Ag/AgCl microelectrodes with tip diameter 0.5 μm were used to measure the plasma membrane potential (MP) of *Arabidopsis* leaf segments. Measurements were taken from at least five individual plants for each treatment. MPs were recorded for at least 10 s after the potential stabilized following cell penetration.

2.14. Leaf K^+ content estimation

0.3 g dry leaf samples were digested in a 120 ml Teflon digestion vessel with 5 ml HNO_3 by using a microwave digester (Mars 6 Microwave Digestion System, CEM Corporation, Matthews, NC, USA). Digested samples were centrifuged at 5000*g* for 10 min at ambient temperature (Avanti J-30I centrifuge, Beckman Coulter, Krefeld, Germany). After centrifugation, 0.2 mL of the digested solution was diluted with ddH_2O to a final volume of 10 ml. K^+ content was then measured using a flame photometer (PFP7, Jenway, UK).

2.15. ATP content determination

Leaf ATP content of plants infiltrated with PNC or buffer was measured using ATP content determination kit (A22066, Thermofisher). Extraction of leaf ATP was conducted by following previously used methods with some modifications.[45,46] Briefly, about 0.1 g leaf sample from PNC or buffer infiltrated plants was grinded with liquid nitrogen by using mortar and pestle. The sample was transferred to a 1.5 ml Eppendorf tube and 1 ml HCl (0.1 M) added and mix thoroughly and put into boiling water for 10 min. After cooling down on ice, samples were centrifuged at 16 000 rpm for 3 min, and the transferred supernatant was centrifuged again. ATP measuring reaction solution (containing 20× reaction buffer, 0.1 M DTT, 10 mM D-luciferin, and 5 mg ml^{-1} firefly luciferase) was mixed according to manufacturer's instruction. The 90 μl reaction solution was added into each well (Costar white 96 well microplate with flat bottom, Corning). Then, 10 μl diluted ATP standard solutions or leaf sample solution were added into each well. Luminescence (emission 560 nm) was measured with Victor 2 plate reader (Wallac) immediately according to manufacturer's protocol.

2.16. Quantitative real-time PCR analysis

PNC-leaves and NNP-leaves from four weeks old *Arabidopsis* (Col-0) plants exposed to 3 days 100 mM NaCl were excised, cut into small segments, and snap frozen in liquid nitrogen. The leaf RNA was extracted and synthesized to cDNA by using Aurum™ Total RNA Mini Kit (Bio-Rad) and iScript RT supermix (one-step cDNA mix, Bio-Rad) following the manufacturer's instruction.[47] Quantitative real-time PCR was performed using a Bio-Rad CFX Connect Real Time Thermal Cycler and SYBR green PCR reagent (Bio-Rad) as described in Vandesompele *et al.*[48] The relative expression level of studied genes was analyzed by $2^{-\Delta\Delta CT}$ method.[49] Primers were designed to determine the expression of *AtGork*,[50] *AtHAK5*,[51] *AtAVP*,[52] *AtNHX1*[52] and *ATAHA1*[52] (see ESI† Table S1 for primer sequences). The control gene (*Actin*[53] and *GAPDH*[54]) was used for normalization of the test gene transcript. Experiments were repeated in three individuals (each biological replicate was measured for four times).

2.17. Statistical analysis

All data were represented as mean ± SE (n = biological replicates) and analyzed using SPSS 23.0. Comparison was performed by independent samples t-test (two tailed) or one-way ANOVA based on Duncan's multiple range test (two tailed). *, **, and *** represent $P < 0.05$, $P < 0.01$ and $P < 0.001$, respectively. Different lower case letters mean the significance at $P < 0.05$.

3. Results and discussion

The underlying mechanisms of how nanoceria catalytic ROS scavenging affects plant physiological processes associated with salinity stress tolerance are not well understood. Herein, we determined that sub 11 nm negatively charged nanoceria improve chlorophyll content, biomass, photosynthesis, and leaf mesophyll K^+ retention in *Arabidopsis* plants under salt stress. We show that PNC catalytic scavenging of hydroxyl radical and its precursor hydrogen peroxide enables higher mesophyll K^+ retention in leaves of plants under salt stress by affecting the activity and gene expression of K^+ channels/transporters (Fig. 1). Leaf mesophyll K^+ retention has been associated with overall salinity stress tolerance in plants.[32,55] K^+ is an essential nutrient for plants that plays an important role in protein synthesis stabilization, enzyme activation, membrane potential formation and maintenance of turgor pressure.[31]

3.1. Enhanced salinity tolerance in *Arabidopsis* plants engineered with nanoceria

Plant tolerance to salt stress was assessed by measuring changes in plant agronomical (shoot biomass) and physiological parameters (chlorophyll content; leaf photosynthetic traits). After three days of 100 mM NaCl, plants infiltrated with PNC were visibly healthier (Fig. 2A) and exhibited higher chlorophyll content levels relative to controls infiltrated with buffer with no nanoparticles (NNP) (SPAD readout, Fig. 2B). We observed enhanced photosystem II quantum yield (QY, up to 30% increase, $P < 0.05$) (Fig. 2C) and higher maximum efficiency of photosystem II (Fv/Fm, 9%, $P < 0.05$, Fig. 2D) in leaves infiltrated with PNC (PNC-leaves) relative to their

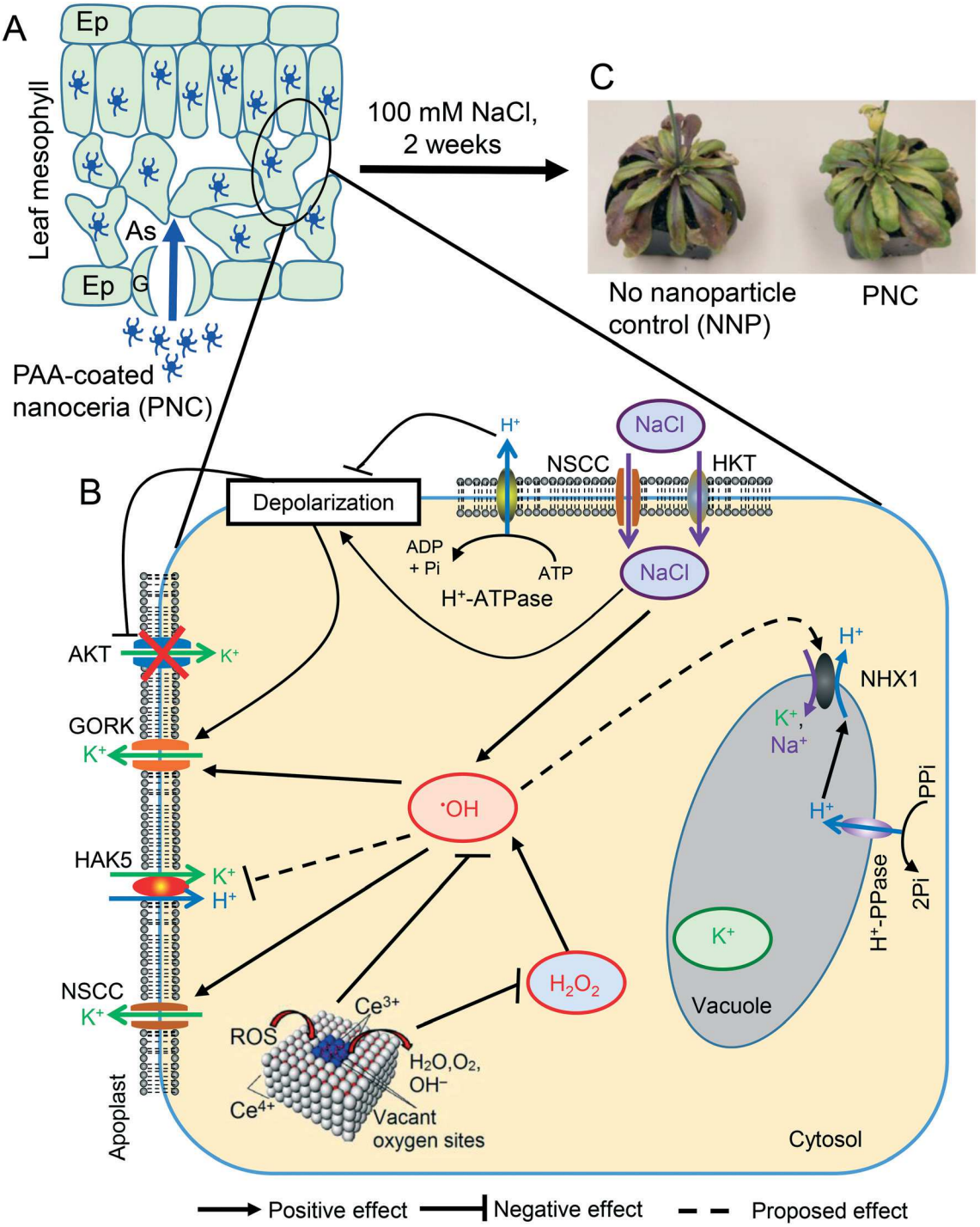

Fig. 1 Model of nanoceria improvement of salt tolerance by enabling higher leaf mesophyll K^+ retention. (A) Polyacrylic acid coated nanoceria (PNC, −17 mV, 10 nm) are delivered to *Arabidopsis* leaf mesophyll cells through stomatal pores. (B) Nanoceria scavenging of hydroxyl radicals ($^{\cdot}OH$) and its precursor hydrogen peroxide (H_2O_2) influences mesophyll K^+ transport under salt stress. Briefly, plant salt stress induces accumulation of ROS *i.e.* $^{\cdot}OH$ that activate ROS-NSCC and GORK K^+ efflux channels. Large Na^+ influx into the cell cytosol also results in GORK channel activation immediately after rapid plasma membrane potential depolarization. However, once the plasma membrane potential is restored, the contribution to K^+ efflux mediated by ROS has a larger impact than that induced by Na^+ influx. Nanoceria act as potent catalytic scavengers of $^{\cdot}OH$ and H_2O_2 alleviating oxidative stress and in turn reducing K^+ efflux and improving K^+ retention. (C) PNC infiltrated *Arabidopsis* plants have higher salt tolerance (100 mM NaCl, two weeks) than controls without nanoparticles. As, air space; Ep, epidermal cell; G, guard cell.

control counterparts without nanoparticles (NNP-leaves). No significant differences in either chlorophyll content index, QY, and Fv/Fm were found between PNC-leaves and NNP-leaves under non-saline conditions (Fig. S2†). The salt

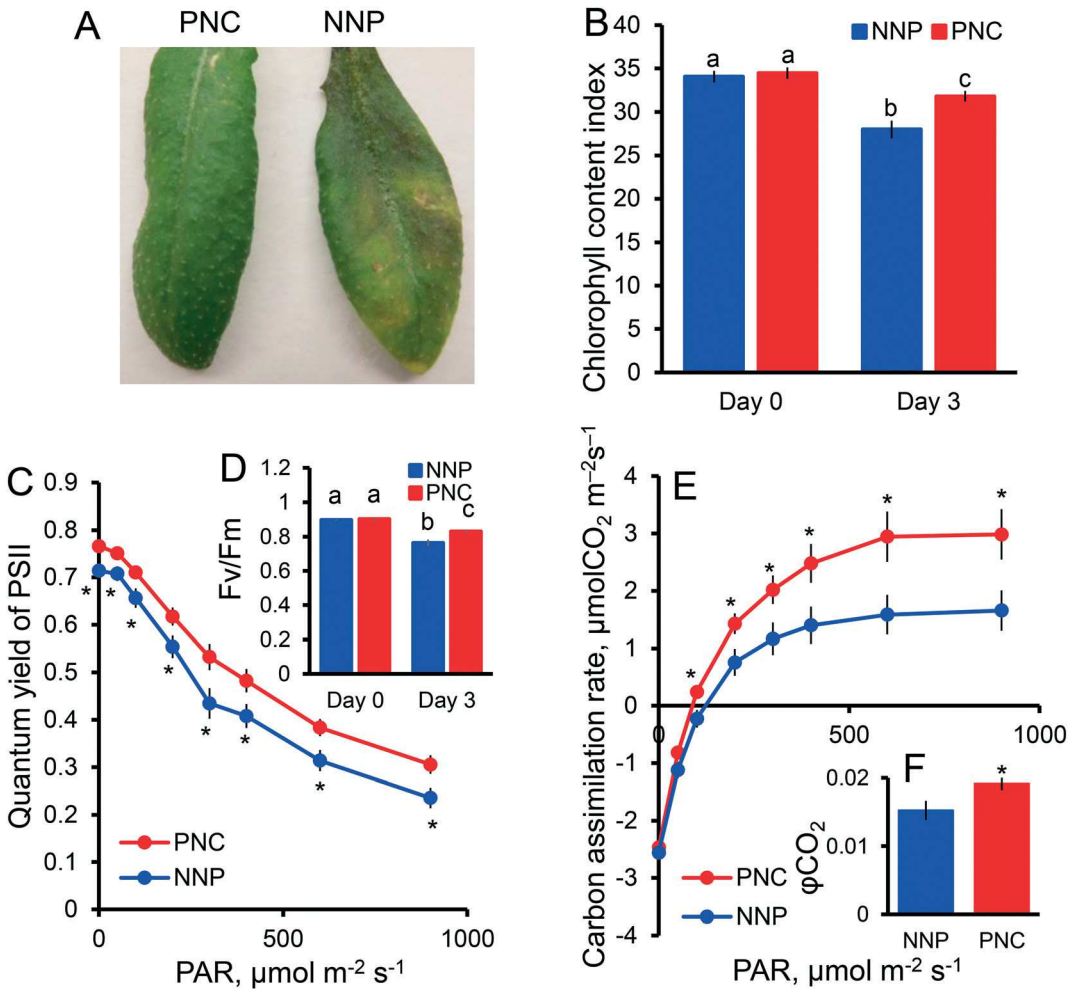

Fig. 2 Improved photosynthetic performance of leaves infiltrated with nanoceria in *Arabidopsis* plants exposed to salinity stress (100 mM NaCl, 3 days). (A and B) Comparison of chlorophyll content in leaves infiltrated with PNC (PNC-leaves) and buffer with no nanoparticles (NNP-leaves) at 0 and 3 days of exposure to 100 mM NaCl. Quantum yield of PS II (QY) (C), maximum quantum yield of PSII (Fv/Fm) (D), carbon assimilation rates (*A*) (E), and quantum efficiency of CO_2 (φ_{CO_2}) (F) of PNC-leaves and NNP-leaves after 3 days, 100 mM NaCl treatment. Mean ± SE (n = 15–16). *, $P < 0.05$. Different lower case letters mean significant differences at $P < 0.05$.

stressed PNC-leaves have increased carbon assimilation rates (*A*, 85%, $P < 0.05$) (Fig. 2E) and quantum efficiency of CO_2 (φ_{CO_2}, 26%, $P < 0.05$) (Fig. 2F) compared to NNP-leaves. These changes in leaf carbon uptake were accompanied by higher stomatal conductance (Gs) in PNC-leaves (up to 38% increase, $P < 0.05$) relative to NNP-leaves under salt stress (Fig. S3†). Negatively charged PNC (51 mg L^{-1}) exhibit high levels of colocalization with *Arabidopsis* leaf mesophyll chloroplasts *in vivo* (46%) where they enhance photosynthesis under abiotic stress by scavenging ROS.[19] PNC also improve shoot biomass (18%, $P < 0.05$) in four week-old plants subjected to 100 mM NaCl for two weeks, relative to plants without nanoparticles (Fig. S4†). Our results are in agreement with a previous study showing that negatively charged nanoceria (zeta potential −51.8 mV, average TEM size 55.6 nm, 1000 mg kg^{-1}) applied to soil alleviates salt stress induced symptoms including reduced leaf biomass, total chlorophyll content, and net carbon assimilation rates in canola plants.[27] In contrast, plant exposure to cerium in the ionic form in $Ce(SO_4)_2$ (0.5–500 mg L^{-1})[20] or $CeCl_3$ (10 mg L^{-1})[56] decreases or has no significant effect on root and shoot biomass. Nanoceria ability to regenerate Ce^{3+} dangling bonds and catalytically scavenge ROS provides *Arabidopsis* plants with sustained alleviation of oxidative stress and enhancement in photosynthetic performance under salt stress.

3.2. ROS catalytic scavenging by nanoceria in salinity stressed leaves

ROS accumulation is a hallmark of abiotic stress in plants. Hydroxyl radical generation *in vivo* was monitored *via* confocal fluorescence microscopy with HPF (hydroxyphenyl fluorescein) dye. HPF remains in a non-fluorescent form until it reacts with $^{\cdot}OH$ or peroxynitrite anion but not other ROS.[57] The high HPF selectivity of 6 : 1 between $^{\cdot}OH$ and peroxynitrite[57] has been used for *in vivo* imaging of $^{\cdot}OH$ in mammalian cells.[58] We conducted *in vitro* nanoceria ROS scavenging experiments that demonstrated PNC effectively reduces levels

of ˙OH generated by Cu/Asc as indicated by the significantly lower fluorescence intensity of HPF dye in samples with PNC relative to buffer without nanoparticles (Fig. 3A). We report a significantly lower HPF dye fluorescence (41%, $P < 0.001$) in PNC-leaves relative to NNP-leaves under salt stress (Fig. 3C and D) indicating efficient scavenging of ˙OH in salt stressed plants by PNC *in vivo*. Hydrogen peroxide, a precursor of ˙OH, was visualized by histochemical staining with DAB (3,3′-diamionbenzidine) of PNC-leaves and NNP-leaves (Fig. 3B). DAB staining clearly showed lower accumulation of H_2O_2 in PNC-leaves than in NNP-leaves after 3 days of salt stress (100 mM NaCl). Confocal imaging of H_2O_2 was conducted using H_2-DCFDA (2′,7′-dichlorodihydrofluorescein diacetate) dye. H_2-DCFDA reaction with ROS, primarily with H_2O_2, leads to conversion into its fluorescent form DCF (2′,7′-dichlorofluorescein). DCF fluorescence intensity in PNC-leaves is 44% lower than that of NNP-leaves after 3 days of salt stress ($P < 0.001$) (Fig. 3B, C, and E). NBT (nitro blue tetrazolium chloride) staining and DHE (dihydroethidium) dye were applied to image superoxide anion (Fig. S5A†), a precursor of H_2O_2. DHE can freely permeate cell membranes and react with superoxide anions to generate its fluorescent form 2-hydroxyethidium.[59] PNC-leaves have 37% less ($P < 0.01$) DHE fluorescence intensity than NNP-leaves after salt stress (Fig. S5B and C†). Nanoceria *in vitro* scavenging of superoxide anion and H_2O_2 has been previously reported.[16,19] The PNC used in this study have low Ce^{3+}/Ce^{4+} ratio (35 ± 2.2%) (Fig. S1†) which has been identified as having CAT and SOD mimetic activity that effectively scavenges ROS.[16,19] Overall, our results demonstrate that PNC significantly lower levels of

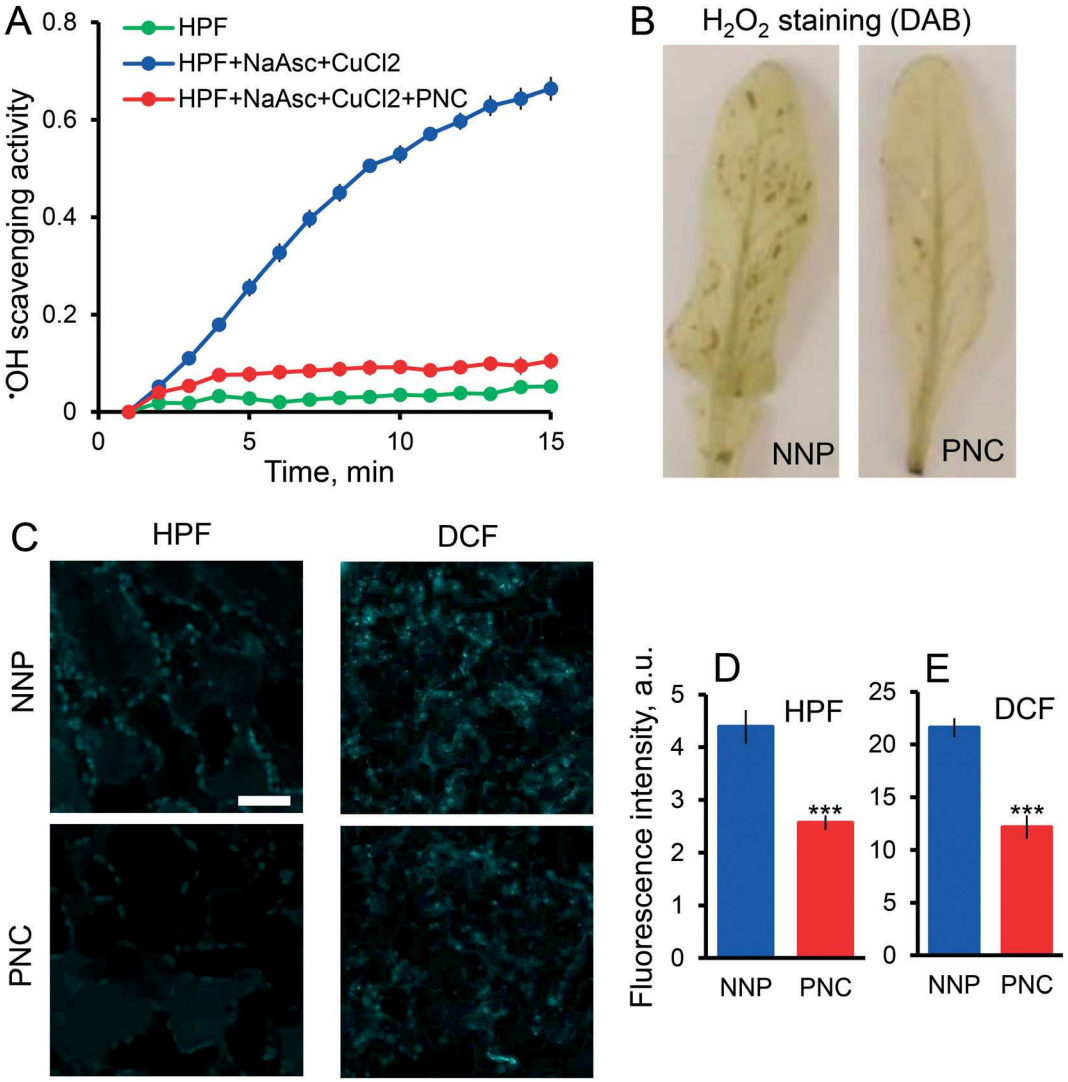

Fig. 3 Catalytic scavenging of hydroxyl radical and hydrogen peroxide by nanoceria *in vitro* and *in vivo* in *Arabidopsis* leaf mesophyll cells under salinity stress (100 mM NaCl, 3 days). (A) PNC efficiently scavenge hydroxyl radicals generated by copper/ascorbate mixture. Hydroxyl radicals were monitored by HPF fluorescent dye. Mean ± SE (n = 3–6). (B) Histochemical staining with DAB (hydrogen peroxide, dark brown spots) of leaves infiltrated with PNC (PNC-leaves) and buffer with no nanoparticles (NNP-leaves) under salt stress. (C) Confocal images of leaf spongy mesophyll cells showing the intensity of hydroxyl radical (HPF) and hydrogen peroxide (DCF). (D and E) Comparison of HPF and DCF intensity between PNC-leaves and NNP-leaves under salt stress. Mean ± SE (n = 3–4). Scale bar represents 40 μm. ***, $P < 0.001$.

$^{\cdot}OH$ and its precursor H_2O_2 in leaves of *Arabidopsis* plants under salt stress.

3.3. Higher K^+ retention in leaf mesophyll cells with embedded nanoceria

Leaf mesophyll K^+ distribution in the vacuole and cytosol was imaged using APG-2 cell permeable fluorescent dye together with FM4-64 for plasma membrane and tonoplast staining. Under salt stress, PNC-leaves exhibit an almost one-fold higher K^+ dye intensity in the cytosol than NNP-leaves (Fig. 4A and B) and K^+ content in whole PNC-leaves is higher than in NNP-leaves (Fig. 4C) indicating that PNC ROS scavenging promotes K^+ mesophyll retention in leaves. No differences in leaf K^+ content were found between plants infiltrated with PNC and buffer solution under control conditions (Fig. 4C). The K^+ dye intensity values were similar in the vacuole of leaf mesophyll cells under salt stress (Fig. 4B). To date, no ROS activated vacuolar K^+ channels or transporters have been reported in leaf mesophyll cells,[60] in agreement with the lack of differences in vacuole K^+ levels between PNC-leaves and NNP-leaves. Non-invasive microelectrode ion flux estimation (MIFE) measurements found that both transient and steady-state NaCl-induced K^+ efflux is higher in NNP-leaves than in PNC-leaves (Fig. 5A). Thus, PNC-leaves have a significantly less K^+ loss than NNP-leaves under salt stress (Fig. 5B). In contrast, no significant differences of NaCl-induced H^+ flux and average H^+ loss were observed between PNC-leaves and NNP-leaves (Fig. 5C and D). Plasma membrane potential is a key plant physiological trait that influences the transport of ions across the cell membrane.[33,43,61–65] This potential is mainly built by H^+-ATPase pumping of H^+ from cytosol to the aploplast.[66] One of the detrimental effects of salinity stress is the

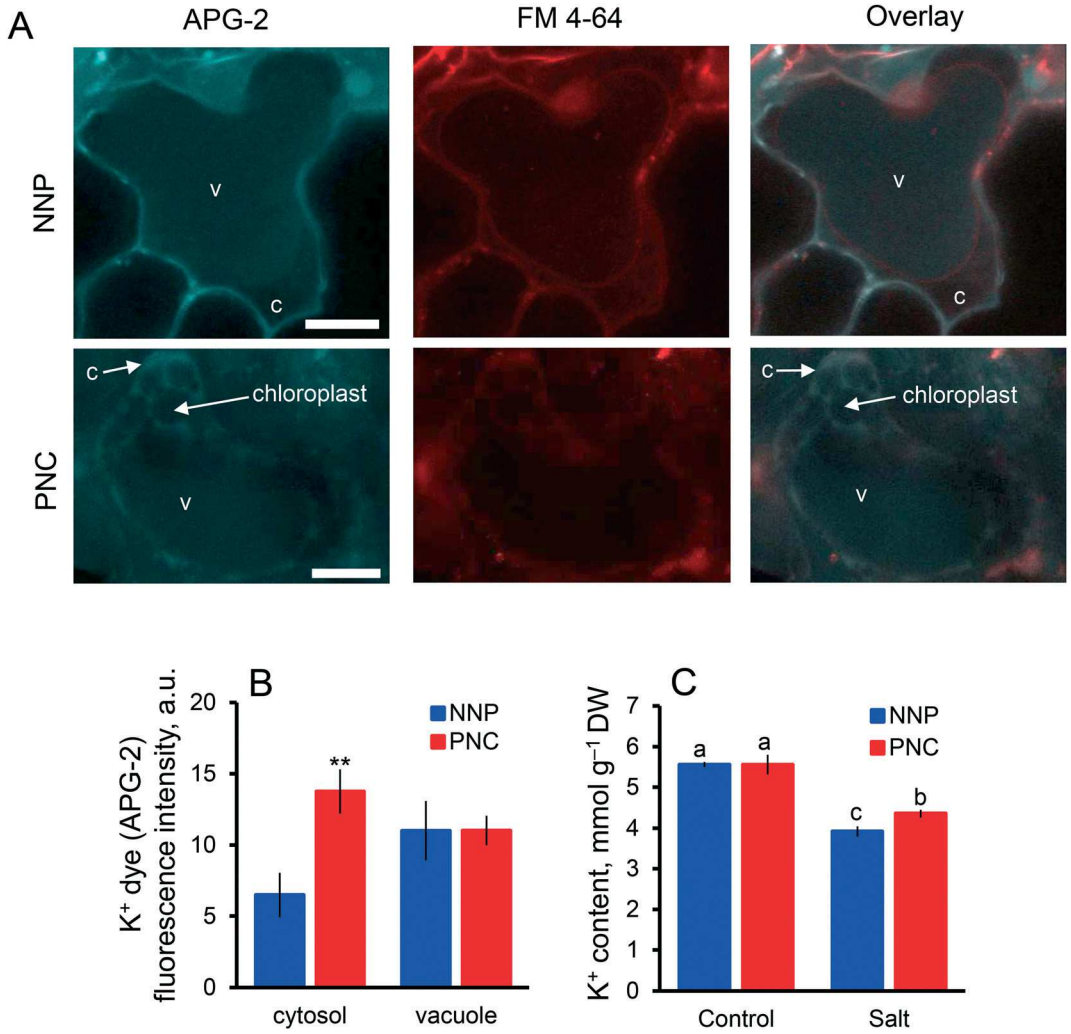

Fig. 4 Higher cytosolic K^+ retention ability in leaf mesophyll cells with embedded nanoceria ROS scavengers in plants under salinity stress (100 mM NaCl, 3 days). (A) Confocal images of K^+ distribution in cytosol (c) and vacuole (v) measured by APG-2 dye in leaves infiltrated with PNC (PNC-leaves) and buffer with no nanoparticles (NNP-leaves). The plasma membrane and tonoplast were stained with FM 4-64. (B) Fluorescence intensity of APG-2 in cytosol and vacuole. Mean ± SE (n = 4). (C) Leaf K^+ content of PNC- and NNP-leaves under salt stress. Mean ± SE (n = 5–6). Scale bar represents 20 μm. **, $P < 0.01$. Different lower case letters mean significant differences at $P < 0.05$.

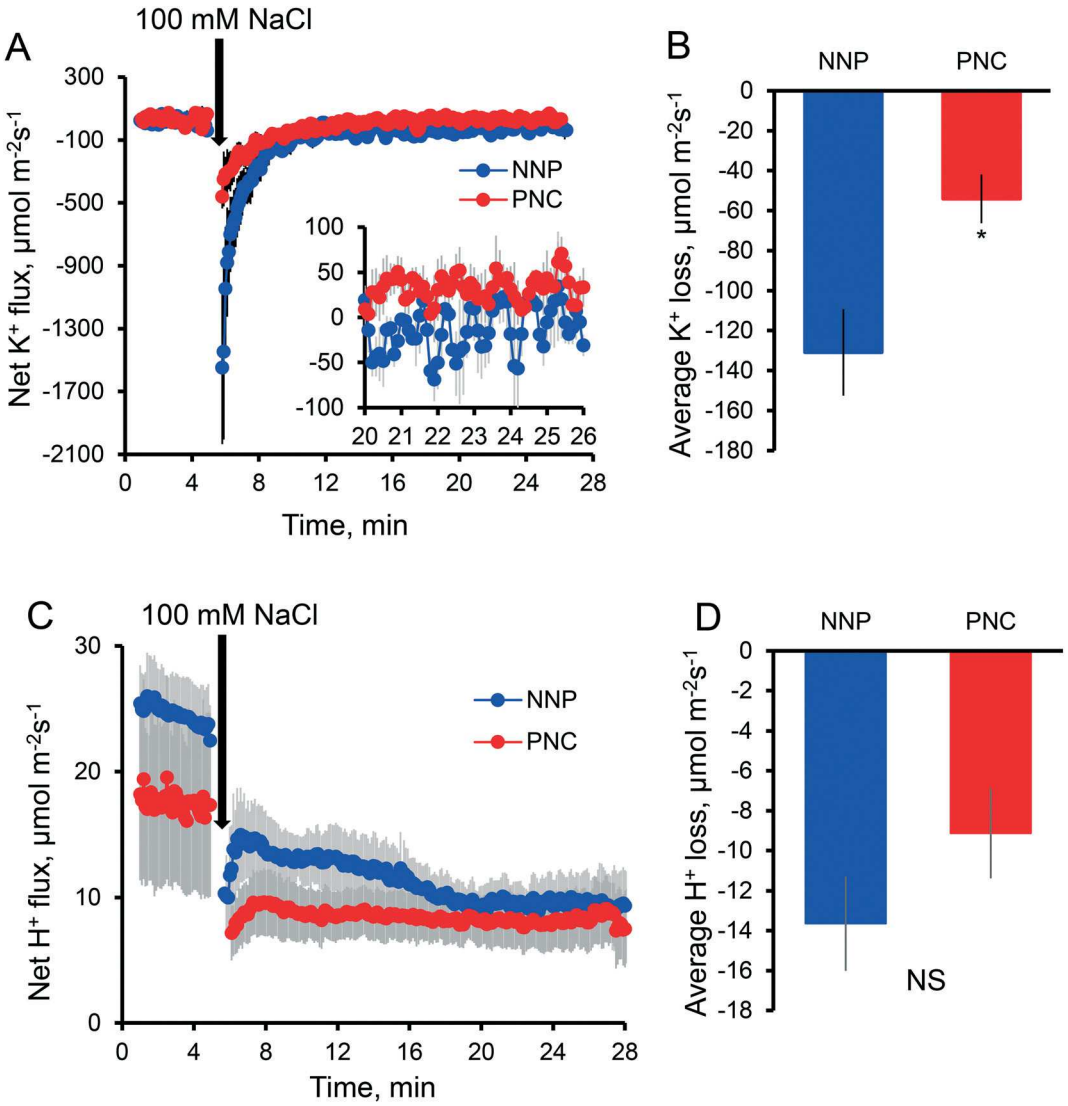

Fig. 5 Nanoceria ROS scavengers reduce leaf mesophyll K^+ efflux without affecting H^+ flux in plants under salt stress (100 mM NaCl, 3 days). NaCl-Induced kinetics of mesophyll K^+ efflux (A), average K^+ loss (B), H^+ flux (C) and average H^+ loss (D) measured by MIFE in leaves infiltrated with PNC (PNC-leaves) and buffer with no nanoparticles (NNP-leaves). Mean ± SE (n = 4–5). *, $P < 0.05$. NS, no significant difference.

depolarization of the plasma membrane potential.[32,67,68] Our results indicate that although PNC enhances K^+ mesophyll retention it does not affect the plasma membrane potential in *Arabidopsis* plants under salt stress.

The effect of nanoparticles *e.g.* nanoceria on the activity of plasma membrane channels/transporters controlling K^+ fluxes is poorly understood. Recently, Sosan *et al.*[69] found that silver nanoparticles slightly inhibit plasma membrane K^+ efflux currents in *Arabidopsis* root cell protoplasts. We measured K^+ fluxes in PNC- and NNP-inoculated leaves in response to ROS accumulation, a secondary stress in plants under high salinity.[70] Hydroxyl radicals were generated by copper/ascorbate (Cu/Asc) mixture and H_2O_2 (30%, Sigma Aldrich) was also tested. A 48% and 45% lower K^+ efflux was observed in PNC-leaves relative to NNP-leaves in the presence of $^{\cdot}OH$ (Cu/Asc solution) (Fig. 6A and C) and in samples treated with H_2O_2, respectively (Fig. 6B and C) ($P < 0.001$). ROS-activated NSCC channel activity can be promoted in the presence of $^{\cdot}OH$ or H_2O_2. However, the K^+ efflux induced by $^{\cdot}OH$ is over ten times higher than that induced by H_2O_2 (-Fig. 6A–C). A high K^+ efflux has also been reported in *Arabidopsis* roots in the presence of $^{\cdot}OH$ (generated by Cu/Asc).[71] Hydrogen peroxide, a precursor of $^{\cdot}OH$, also stimulates K^+ efflux in *Arabidopsis* roots likely by reacting with transition metals to form $^{\cdot}OH$.[34] Furthermore, samples pretreated with Gd^{3+}, a blocker for NSCC, showed over 90% blockage of $^{\cdot}OH$ induced K^+ efflux in leaf mesophyll cells (Fig. 6D and E). Application of TEA (tetraethylammonium), a GORK channel inhibitor, was much less efficient (~50% inhibition of K^+ efflux in the presence of $^{\cdot}OH$) (Fig. 6D). However, both plasma membrane potential depolarization (gating factors that trigger GORK channel activation and a consequent K^+ efflux) and net H^+ effluxes were similar between PNC-inoculated and NNP-inoculated leaves under salt stress

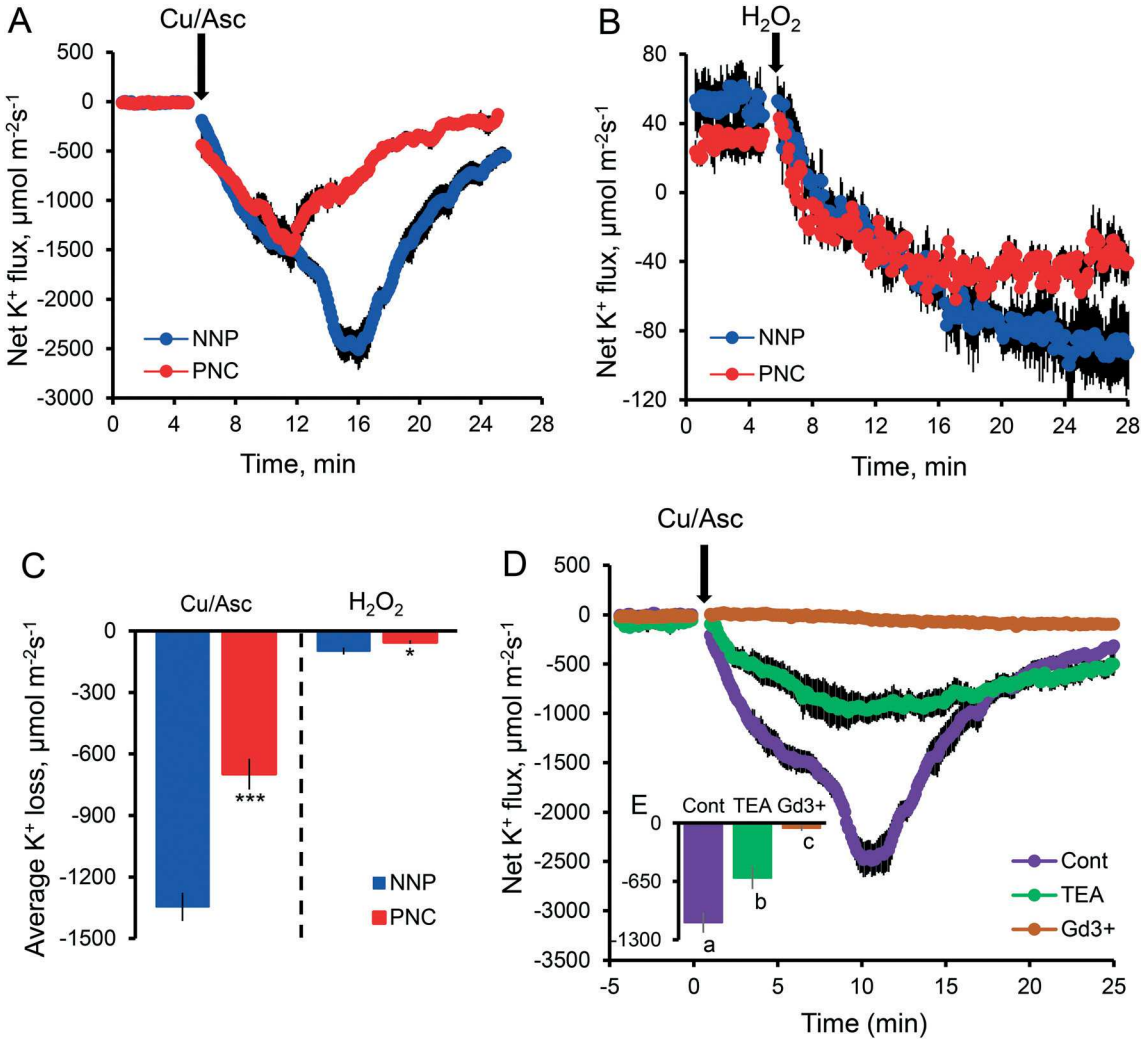

Fig. 6 Hydroxyl radical scavenging by nanoceria improves mesophyll K^+ retention *via* NSCC channels. (A and B) Kinetics of mesophyll K^+ efflux induced by hydroxyl radicals (generated by Cu/Asc, 0.3 mM/1 mM) and hydrogen peroxide (10 mM) in leaves infiltrated with PNC (PNC-leaves) and buffer with no nanoparticles (NNP). (C) Average K^+ loss from mesophyll induced by hydroxyl radicals (generated by Cu/Asc mix) and hydrogen peroxide in leaves infiltrated with PNC (PNC-leaves) and buffer with no nanoparticles (NNP). (D and E) K^+ efflux and average K^+ loss from leaf mesophyll in the presence of channel blocker of NSCC channels (Gd^{3+}) and GORK channel inhibitor (TEA). Mean ± SE (n = 6–11). *, $P < 0.05$; ***, $P < 0.001$. Different lower case letters mean significant differences at $P < 0.05$.

(Fig. 5C and D and 7A). Together, our pharmacological studies indicate that ROS-NSCC but not GORK channels are major contributors to the $^{\cdot}OH$ induced K^+ efflux in mesophyll cells. Improved K^+ retention is mainly achieved by PNC scavenging of $^{\cdot}OH$ but not H_2O_2 or superoxide anion. As it has been reported in roots,[34] $^{\cdot}OH$ exerts the strongest modulation of the activities of ROS-activated NSCC and GORK channels in leaves (Fig. 6). To assess the impact of nanoceria ROS scavenging on the contribution of ATP dependent K^+/H^+ symporters *e.g.*, HAK5 in mesophyll K^+ retention, we measured whole leaf ATP content. However, we found no differences in ATP levels between PNC- and NNP-inoculated leaves under salt stress (Fig. 7B).

ROS accumulation is a well-known secondary stress accompanying salt stress in plants.[70] PNC reduce accumulation of ROS in plants under salt stress including $^{\cdot}OH$ that cannot be scavenged by any known enzymes (Fig. 3A, C, and D and 6). Cerium oxide nanoparticles have been reported to scavenge $^{\cdot}OH$ *in vitro*.[13] In this study, *Arabidopsis* PNC-leaves have 41% lower HPF intensity, an indicator of $^{\cdot}OH$, than control NNP-leaves under salinity stress. PNC-leaves also have 48% lower $^{\cdot}OH$-induced K^+ efflux than NNP-leaves (Fig. 6A). ROS homeostasis is crucial for maintaining K^+ mesophyll retention, a key trait for plant salt tolerance.[30–32,72] In plant root cells under salt stress, $^{\cdot}OH$ is known to activate GORK and NSCC channels leading to increased K^+ efflux in plants root cells.[33,34,73] Here we report that $^{\cdot}OH$ induced leaf mesophyll K^+ efflux is over 10 times higher than that generated by H_2O_2 (Fig. 6). The K^+ efflux induced by H_2O_2 might be due to conversion of H_2O_2 to $^{\cdot}OH$ by cell-wall transition metals and ascorbate.[74,75] We assessed the direct impact of $^{\cdot}OH$ on mesophyll K^+ retention and whether ROS-NSCC or GORK

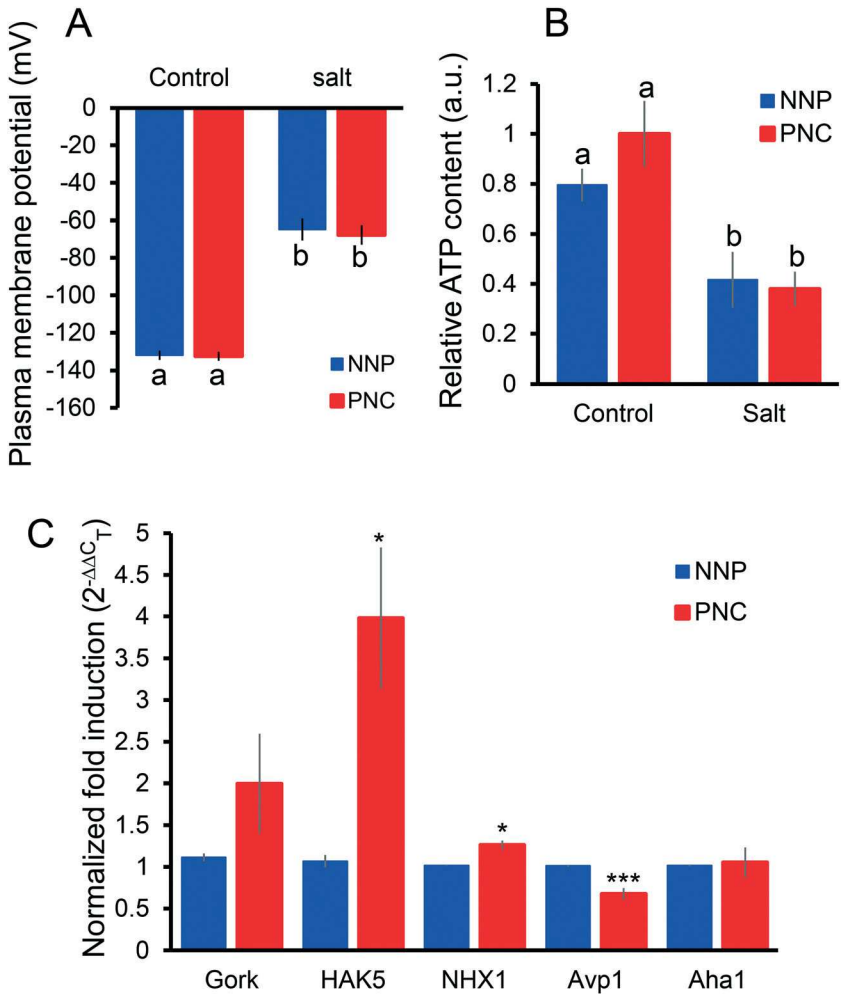

Fig. 7 Effect of PNC on plasma membrane potential, ATP content, and relative expression of K^+ channel/transporter genes in *Arabidopsis* leaves under salt stress. (A) Plasma membrane potential in leaves infiltrated with PNC and buffer with no nanoparticles (NNP) in response to salt stress. Mean ± SE (n = 5–7). (B) ATP content in PNC-leaves and NNP-leaves after salt stress. Mean ± SE (n = 4). (C) Relative expression of K^+ channel/transporter genes in the plasma membrane and tonoplast of *Arabidopsis* leaves (Col-0) under 100 mM NaCl treatment for 3 days. Mean ± SE (n = 3). *, $P < 0.05$; ***, $P < 0.001$. Different lower case letters mean significant differences at $P < 0.05$.

channels play a main role in controlling $^{\cdot}OH$-induced K^+ efflux. Our results indicate that $^{\cdot}OH$ can induce a significant K^+ efflux in *Arabidopsis* leaf mesophyll, and ROS-activated NSCC channels but not GORK channel play a major role in this process (Fig. 6 and 7). Besides its role in elongation/expansion of plant cells,[35,76] ROS-activated NSCC channels are known to be involved in NaCl-induced K^+ efflux in root[77] and mesophyll[78] cells. Overall, our results indicate that PNC augmented $^{\cdot}OH$ scavenging modulates activities of ROS-activated NSCC and GORK channels and reduces K^+ loss from cytosol, thus improving plant salinity stress tolerance.

3.4. Nanoceria effect on K^+ channel and transporter transcription levels in leaves

To further understand the effect of nanoceria on K^+ mesophyll transport in leaves of *Arabidopsis* plants under salt stress, we assessed the relative gene expression of a set of channels/transporters involved in K^+ transport. No significant changes in relative gene expression of *gork* were found between PNC-leaves and NNP-leaves under salt stress (Fig. 7C). The K^+ influx symporter *HAK5* gene was significantly upregulated in PNC-leaves (Fig. 7C). HAK/KUP is a family of symporters that are key in K^+ uptake of plants under salt stress. Although *HAK5* gene encoding K^+/H^+ symporter was upregulated, its co-transport activity is dependent on the H^+ electrochemical gradient across plasma membrane that requires ATP. The generation of ATP is well known to be reduced in plants under salt stress.[79,80] We recorded a 50% drop of ATP content in leaves under salt stress (Fig. 7B) but no differences in the ATP content between PNC- and NNP-inoculated leaves. Thus, HAK5 active transporter contribution to K^+ retention is not expected to be significant compared to NSCC and GORK channels due to low ATP levels (Fig. 7B). Relative gene expression of H^+-ATPase (Fig. 7C) and net H^+ efflux (Fig. 5C and D) in PNC-leaves were similar to NNP-leaves under salt stress. H^+-ATPase pumps H^+ from the cell cytosol to the extra cellular space (apoplast), building up the

electrochemical gradient that forms the plasma membrane potential.[66] Plasma membrane depolarization occurs immediately after onset of salt stress in plants.[68] Here we found that the degree of plasma membrane potential depolarization in PNC-leaves was also similar to NNP-leaves (Fig. 7A). Thus improved mesophyll K^+ retention was unlikely due to lower depolarization of the plasma membrane potential enabled by PNC ROS scavenging under salt stress. The *NHX1* gene (a tonoplast K^+, Na^+/H^+ antiporter) was upregulated whereas the relative expression of *Avp* gene (a tonoplast PPase-driven hydrogen pump which fuels the NHX1 antiporter)[81] was downregulated in PNC-leaves relative to NNP-leaves under salt stress (Fig. 7C). Therefore the import of K^+ through NHX1 from cytosol to vacuole[82] might be compromised by the lower H^+ electrochemical gradient provided by H^+-PPase. In accordance with these results, no significant differences were found in the vacuole APG-2 (K^+ dye) intensity between PNC-leaves and NNP-leaves under high salinity (Fig. 4B). Relative expression of proton pump *Aha* gene was not significantly different between PNC- and NNP-inoculated leaves under salt stress (Fig. 7C).

4. Conclusion

Maintaining plant cell K^+ retention is regarded as a mechanism to improve salinity stress tolerance in crops.[83] In this study, we show that PNC scavenging of $^{\bullet}OH$ and its precursors leads to higher leaf mesophyll K^+ retention under salinity stress. PNC increase photosynthetic carbon assimilation rates and quantum yield of PSII, and shoot biomass in *Arabidopsis* under salinity stress. PNC ability to localize inside plant cells and catalytically reducing $^{\bullet}OH$ (Fig. 3) is a key tool for understanding the role of ROS in plant stress responses and elucidate plant–nanoceria interactions. Like hydrogen peroxide, $^{\bullet}OH$ has been proposed to have a dual role in plant physiology acting as harmful molecules at high levels and being involved in stress signaling at low concentration.[84–87] However, current chemical based tools for *in vivo* $^{\bullet}OH$ scavenging[88–90] cannot sustain long term catalytic scavenging as nanoceria. Herein, we show that PNC catalytic scavenging of $^{\bullet}OH$ strongly influences the activity of ROS-NSCC and GORK channels in plant leaves, key plasma membrane channels controlling plant cell K^+ retention. To meet the food demand for the projected 9.3 billion human population at 2050, agricultural production needs to be increased by 60% from the 2005–2007 level.[91] Land salinization is a main limitation for agricultural production worldwide[92] that is being exacerbated by a changing climate[93] and utilization of fertilizers[94] resulting in multi-billion dollar annual losses.[95] Scalable and economical foliar spray delivery methods of PNC may alleviate oxidative stress and mesophyll K^+ loss caused by salt stress and improve crop growth and yield.

Conflicts of interest

The authors declare no competing financial interest.

Acknowledgements

This material is based upon work supported by the National Science Foundation under Grant No. 1817363 to J. P. G. This work was supported by the University of California, Riverside and USDA National Institute of Food and Agriculture, Hatch project 1009710 to J. P. G. and ARC (DPDP150101663) and GRDC grants (UT00027) to S. S.

References

1 A. Fita, A. Rodríguez-Burruezo, M. Boscaiu, J. Prohens and O. Vicente, Breeding and domesticating crops adapted to drought and salinity: A new paradigm for increasing food production, *Front. Plant Sci.*, 2015, **6**, 978.
2 R. Munns and M. Tester, Mechanisms of salinity tolerance, *Annu. Rev. Plant Biol.*, 2008, **59**, 651–681.
3 V. Demidchik, Mechanisms of oxidative stress in plants: From classical chemistry to cell biology, *Environ. Exp. Bot.*, 2015, **109**, 212–228.
4 S. S. Gill and N. Tuteja, Reactive oxygen species and antioxidant machinery in abiotic stress tolerance in crop plants, *Plant Physiol. Biochem.*, 2010, **48**, 909–930.
5 Y. G. Song, B. Liu, L. F. Wang, M. H. Li and Y. Liu, Damage to the oxygen-evolving complex by superoxide anion, hydrogen peroxide, and hydroxyl radical in photoinhibition of photosystem II, *Photosynth. Res.*, 2006, **90**, 67–78.
6 H. Sies, Strategies of antioxidant defense, *Eur. J. Biochem.*, 1993, **215**, 213–219.
7 K. Das and A. Roychoudhury, Reactive oxygen species (ROS) and response of antioxidants as ROS-scavengers during environmental stress in plants, *Front. Environ. Sci.*, 2014, **2**, 1–13.
8 J. P. Giraldo, M. P. Landry, S. M. Faltermeier, T. P. McNicholas, N. M. Iverson, A. A. Boghossian, N. F. Reuel, A. J. Hilmer, F. Sen, J. A. Brew and M. S. Strano, Plant nanobionics approach to augment photosynthesis and biochemical sensing, *Nat. Mater.*, 2014, **13**, 400–408.
9 W. Du, W. Tan, J. R. Peralta-Videa, J. L. Gardea-Torresdey, R. Ji, Y. Yin and H. Guo, Interaction of metal oxide nanoparticles with higher terrestrial plants: Physiological and biochemical aspects, *Plant Physiol. Biochem.*, 2017, **110**, 210–225.
10 A. Pérez-de-Luque, Interaction of nanomaterials with plants: What do we need for real applications in agriculture?, *Front. Environ. Sci.*, 2017, **5**, 1–7.
11 P. Wang, E. Lombi, F. J. Zhao and P. M. Kopittke, Nanotechnology: A new opportunity in plant sciences, *Trends Plant Sci.*, 2016, **21**, 699–712.
12 M. H. Wong, J. P. Giraldo, S. Y. Kwak, V. B. Koman, R. Sinclair, T. T. S. Lew, G. Bisker, P. Liu and M. S. Strano, Nitroaromatic detection and infrared communication from wild-type plants using plant nanobionics, *Nat. Mater.*, 2017, **16**, 264–272.
13 Y. Xue, Q. Luan, D. Yang, X. Yao and K. Zhou, Direct evidence for hydroxyl radical scavenging activity of cerium oxide nanoparticles, *J. Phys. Chem. C*, 2011, **115**, 4433–4438.

14 B. Nelson, M. Johnson, M. Walker, K. Riley and C. Sims, Antioxidant cerium oxide nanoparticles in biology and medicine, *Antioxidants*, 2016, **5**, 15.
15 C. Walkey, S. Das, S. Seal, J. Erlichman, K. Heckman, L. Ghibelli, E. Traversa, J. F. McGinnis and W. T. Self, Catalytic properties and biomedical applications of cerium oxide nanoparticles, *Environ. Sci.: Nano*, 2015, **2**, 33–53.
16 G. Pulido-Reyes, I. Rodea-Palomares, S. Das, T. S. Sakthivel, F. Leganes, R. Rosal, S. Seal and F. Fernández-Piñas, Untangling the biological effects of cerium oxide nanoparticles: the role of surface valence states, *Sci. Rep.*, 2015, **5**, 15613.
17 P. Dutta, S. Pal, M. S. Seehra, Y. Shi, E. M. Eyring and R. D. Ernst, Concentration of Ce^{3+} and oxygen vacancies in cerium oxide nanoparticles, *Chem. Mater.*, 2006, **18**, 5144–5146.
18 A. A. Boghossian, F. Sen, B. M. Gibbons, S. Sen, S. M. Faltermeier, J. P. Giraldo, C. T. Zhang, J. Zhang and M. S. Strano, Application of nanoparticle antioxidants to enable hyperstable chloroplasts for solar energy harvesting, *Adv. Energy Mater.*, 2013, **3**, 881–893.
19 H. Wu, N. Tito and J. P. Giraldo, Anionic cerium oxide nanoparticles protect plant photosynthesis from abiotic stress by scavenging reactive oxygen species, *ACS Nano*, 2017, **11**, 11283–11297.
20 S. D. Ebbs, S. J. Bradfield, P. Kumar, J. C. White, C. Musante and X. Ma, Accumulation of zinc, copper, or cerium in carrot (*Daucus carota*) exposed to metal oxide nanoparticles and metal ions, *Environ. Sci.: Nano*, 2016, **3**, 114–126.
21 C. M. Rico, M. G. Johnson, M. A. Marcus and C. P. Andersen, Intergenerational responses of wheat (*Triticum aestivum* L.) to cerium oxide nanoparticles exposure, *Environ. Sci.: Nano*, 2017, **4**, 700–711.
22 E. Spielman-Sun, E. Lombi, E. Donner, D. Howard, J. M. Unrine and G. V. Lowry, Impact of surface charge on cerium oxide nanoparticle uptake and translocation by wheat (*Triticum aestivum*), *Environ. Sci. Technol.*, 2017, **51**, 7361–7368.
23 L. Pagano, F. Pasquali, S. Majumdar, R. De la Torre-Roche, N. Zuverza-Mena, M. Villani, A. Zappettini, R. E. Marra, S. M. Isch, M. Marmiroli, E. Maestri, O. P. Dhankher, J. C. White and N. Marmiroli, Exposure of Cucurbita pepo to binary combinations of engineered nanomaterials: physiological and molecular response, *Environ. Sci.: Nano*, 2017, **4**, 1579–1590.
24 L. Rossi, H. Sharifan, W. Zhang, A. P. Schwab and X. Ma, Mutual effects and in-planta accumulation of co-existing cerium oxide nanoparticles and cadmium in hydroponically grown soybean (*Glycine max* (L.) Merr.), *Environ. Sci.: Nano*, 2018, **5**, 150–157.
25 C. Ma, H. Liu, H. Guo, C. Musante, S. H. Coskun, B. C. Nelson, J. C. White, B. Xing and O. P. Dhankher, Defense mechanisms and nutrient displacement in *Arabidopsis thaliana* upon exposure to CeO_2 and In_2O_3 nanoparticles, *Environ. Sci.: Nano*, 2016, **3**, 1369–1379.
26 D. Cui, P. Zhang, Y. Ma, X. He, Y. Li, J. Zhang, Y. Zhao and Z. Zhang, Effect of cerium oxide nanoparticles on asparagus lettuce cultured in an agar medium, *Environ. Sci.: Nano*, 2014, **1**, 459–465.
27 L. Rossi, W. Zhang, L. Lombardini and X. Ma, The impact of cerium oxide nanoparticles on the salt stress responses of Brassica napus L, *Environ. Pollut.*, 2016, **219**, 28–36.
28 Z. Cao, C. Stowers, L. Rossi, W. Zhang, L. Lombardini and X. Ma, Physiological effects of cerium oxide nanoparticles on the photosynthesis and water use efficiency of soybean (*Glycine max* (L.) Merr.), *Environ. Sci.: Nano*, 2017, **4**, 1086–1094.
29 I. Hussain, N. B. Singh, A. Singh, H. Singh, S. C. Singh and V. Yadav, Exogenous application of phytosynthesized nanoceria to alleviate ferulic acid stress in Solanum lycopersicum, *Sci. Hortic.*, 2017, **214**, 158–164.
30 H. Wu, L. Shabala, M. Zhou and S. Shabala, Durum and bread wheat differ in their ability to retain potassium in leaf mesophyll: Implications for salinity stress tolerance, *Plant Cell Physiol.*, 2014, **55**, 1749–1762.
31 H. Wu, M. Zhu, L. Shabala, M. Zhou and S. Shabala, K^+ retention in leaf mesophyll, an overlooked component of salinity tolerance mechanism: A case study for barley, *J. Integr. Plant Biol.*, 2015, **57**, 171–185.
32 H. Wu, L. Shabala, K. Barry, M. Zhou and S. Shabala, Ability of leaf mesophyll to retain potassium correlates with salinity tolerance in wheat and barley, *Physiol. Plant.*, 2013, **149**, 515–527.
33 V. Demidchik and F. J. M. Maathuis, Physiological roles of nonselective cation channels in plants: from salt stress to signalling and development, *New Phytol.*, 2007, **175**, 387–404.
34 V. Demidchik, T. A. Cuin, D. Svistunenko, S. J. Smith, A. J. Miller, S. Shabala, A. Sokolik and V. Yurin, *Arabidopsis* root K^+-efflux conductance activated by hydroxyl radicals: single-channel properties, genetic basis and involvement in stress-induced cell death, *J. Cell Sci.*, 2010, **123**, 1468–1479.
35 V. Demidchik, S. N. Shabala, K. B. Coutts, M. A. Tester and J. M. Davies, Free oxygen radicals regulate plasma membrane Ca^{2+}- and K^+-permeable channels in plant root cells, *J. Cell Sci.*, 2003, **116**, 81–88.
36 I. Zepeda-Jazo, A. M. Velarde-Buendia, R. Enriquez-Figueroa, J. Bose, S. Shabala, J. Muniz-Murguia and I. I. Pottosin, Polyamines interact with hydroxyl radicals in activating Ca^{2+} and K^+ transport across the root epidermal plasma membranes, *Plant Physiol.*, 2011, **157**, 2167–2180.
37 M. Safi, H. Sarrouj, O. Sandre, N. Mignet and J. F. Berret, Interactions between sub-10-nm iron and cerium oxide nanoparticles and 3T3 fibroblasts: the role of the coating and aggregation state, *Nanotechnology*, 2010, **21**, 145103.
38 H. Wu, I. Santana, J. Dansie and J. P. Giraldo, *In vivo* delivery of nanoparticles into plant leaves, *Curr. Protoc. Chem. Biol.*, 2017, **9**, 269–284.
39 H. Shi, H. Shi, L. Xiong, L. Xiong, B. Stevenson, B. Stevenson, T. Lu, T. Lu, J. Zhu and J. Zhu, The *Arabidopsis* salt overly sensitive 4 mutants uncover a critical role for vitamin B6 in plant salt tolerance, *Plant Cell*, 2002, **14**, 575–588.

40 H. Shi, M. Ishitani, C. Kim and J. K. Zhu, The *Arabidopsis* thaliana salt tolerance gene SOS1 encodes a putative Na^+/H^+ antiporter, *Proc. Natl. Acad. Sci. U. S. A.*, 2000, **97**, 6896–6901.

41 J. Bose, Y. Xie, W. Shen and S. Shabala, Haem oxygenase modifies salinity tolerance in *Arabidopsis* by controlling K^+ retention via regulation of the plasma membrane H^+-ATPase and by altering SOS1 transcript levels in roots, *J. Exp. Bot.*, 2013, **64**, 471–481.

42 D. Kumar, M. A. Yusuf, P. Singh, M. Sardar and N. B. Sarin, Modulation of antioxidant machinery in α-tocopherol-enriched transgenic Brassica juncea plants tolerant to abiotic stress conditions, *Protoplasma*, 2013, **250**, 1079–1089.

43 S. Shabala, V. Demidchik, L. Shabala, T. A. Cuin, S. J. Smith, A. J. Miller, J. M. Davies and I. A. Newman, Extracellular Ca^{2+} ameliorates NaCl-induced K^+ loss from *Arabidopsis* root and leaf cells by controlling plasma membrane K^+-permeable channels, *Plant Physiol.*, 2006, **141**, 1653–1665.

44 I. A. Newman, Ion transport in roots: measurement of fluxes using ion-selective microelectrodes to characterize transporter function, *Plant, Cell Environ.*, 2001, **24**, 1–14.

45 F. Zeng, L. Shabala, M. Zhou, G. Zhang and S. Shabala, Barley responses to combined waterlogging and salinity stress: separating effects of oxygen deprivation and elemental toxicity, *Front. Plant Sci.*, 2013, **4**, 1–13.

46 D. F. Gaff and H. Ziegler, ATP and ADP contents in leaves of drying and rehydrating desiccation tolerant plants, *Oecologia*, 1989, **78**, 407–410.

47 G. Brychkova, Z. Xia, G. Yang, Z. Yesbergenova, Z. Zhang, O. Davydov, R. Fluhr and M. Sagi, Sulfite oxidase protects plants against sulfur dioxide toxicity, *Plant J.*, 2007, **50**, 696–709.

48 J. Vandesompele, K. De Preter, F. Pattyn, B. Poppe, N. Van Roy, A. De Paepe and F. Speleman, Accurate normalization of real-time quantitative RT-PCR data by geometric averaging of multiple internal control genes, *Genome Biol.*, 2002, **3**, research0034.

49 K. J. Livak and T. D. Schmittgen, Analysis of relative gene expression data using real-time quantitative PCR and the $2^{-\Delta\Delta CT}$ method, *Methods*, 2001, **25**, 402–408.

50 Y. Xie, Y. Mao, W. Zhang, D. Lai, Q. Wang and W. Shen, Reactive oxygen species-dependent nitric oxide production contributes to hydrogen-promoted stomatal closure in *Arabidopsis*, *Plant Physiol.*, 2014, **165**, 759–773.

51 M. Nieves-Cordones, F. Alemán, V. Martínez and F. Rubio, The *Arabidopsis* thaliana HAK5 K^+ transporter is required for plant growth and K^+ acquisition from low K^+ solutions under saline conditions, *Mol. Plant*, 2010, **3**, 326–333.

52 D. H. Oh, S. Y. Lee, R. A. Bressan, D. J. Yun and H. J. Bohnert, Intracellular consequences of SOS1 deficiency during salt stress, *J. Exp. Bot.*, 2010, **61**, 1205–1213.

53 R. A. Volkov, I. I. Panchuk and F. Schöffl, Heat-stress-dependency and developmental modulation of gene expression: The potential of house-keeping genes as internal standards in mRNA expression profiling using real-time RT-PCR, *J. Exp. Bot.*, 2003, **54**, 2343–2349.

54 S. J. Coon, M. Gilliham, A. Athman, A. W. Schreiber, T. Baumann, I. Moller, N. H. Cheng, M. A. Stancombe, K. D. Hirschi, A. A. R. Webb, R. Burton, B. N. Kaiser, S. D. Tyerman and R. A. Leigh, Cell-specific vacuolar calcium storage mediated by CAX1 regulates apoplastic calcium concentration, gas exchange, and plant productivity in *Arabidopsis*, *Plant Cell*, 2011, **23**, 240–257.

55 W. W. Zhang, J. J. Meng, J. Y. Xing, S. Yang, F. Guo, X. G. Li and S. B. Wan, The K^+/H^+antiporter AhNHX1 improved tobacco tolerance to NaCl stress by enhancing K^+ retention, *J. Plant Biol.*, 2017, **60**, 259–267.

56 W. Zhang, S. D. Ebbs, C. Musante, J. C. White, C. Gao and X. Ma, Uptake and accumulation of bulk and nanosized cerium oxide particles and ionic cerium by radish (*Raphanus sativus* L.), *J. Agric. Food Chem.*, 2015, **63**, 382–390.

57 K. Setsukinai, Y. Urano, K. Kakinuma, H. J. Majima and T. Nagano, Development of novel fluorescence probes that can reliably detect reactive oxygen species and distinguish specific species, *J. Biol. Chem.*, 2003, **278**, 3170–3175.

58 M. Price, J. J. Reiners, A. M. Santiago and D. Kessel, Monitoring singlet oxygen and hydroxyl radical formation with fluorescent probes during photodynamic therapy, *Photochem. Photobiol.*, 2009, **85**, 1177–1181.

59 H. Zhao, J. Joseph, H. M. Fales, E. A. Sokoloski, R. L. Levine, J. Vasquez-Vivar and B. Kalyanaraman, Detection and characterization of the product of hydroethidine and intracellular superoxide by HPLC and limitations of fluorescence, *Proc. Natl. Acad. Sci. U. S. A.*, 2005, **102**, 5727–5732.

60 V. Demidchik, ROS-activated ion channels in plants: Biophysical characteristics, physiological functions and molecular nature, *Int. J. Mol. Sci.*, 2018, **19**, 1263.

61 S. Shabala, Signalling by potassium: Another second messenger to add to the list?, *J. Exp. Bot.*, 2017, **68**, 4003–4007.

62 L. Shabala, J. Zhang, I. Pottosin, J. Bose, M. Zhu, A. T. Fuglsang, A. Velarde-Buendia, A. Massart, C. B. Hill, U. Roessner, A. Bacic, H. Wu, E. Azzarello, C. Pandolfi, M. Zhou, C. Poschenrieder, S. Mancuso and S. Shabala, Cell-type-specific H^+-ATPase activity in root tissues enables K^+ retention and mediates acclimation of barley (*Hordeum vulgare*) to salinity stress, *Plant Physiol.*, 2016, **172**, 2445–2458.

63 P. C. Sijmons, F. C. Lanfermeijer, A. H. de Boer, H. B. Prins and H. F. Bienfait, Depolarization of cell membrane potential during trans-plasma membrane electron transfer to extracellular electron acceptors in iron-deficient roots of Phaseolus vulgaris L., *Plant Physiol.*, 2014, **76**, 943–946.

64 C. I. Ullrich and A. J. Novacky, Extra- and intracellular pH and membrane potential changes induced by K^+, Cl^-, $H_2PO_4^-$, and NO_3^- uptake and fusicoccin in root hairs of Limnobium stoloniferum, *Plant Physiol.*, 1990, **94**, 1561–1567.

65 A. Conde, M. M. Chaves and H. Gerós, Membrane transport, sensing and signaling in plant adaptation to environmental stress, *Plant Cell Physiol.*, 2011, **52**, 1583–1602.

66 M. G. Palmgren, Plant plasma membrane H^+-ATPases, *Annu. Rev. Plant Biol.*, 2001, **52**, 817–845.
67 Z. Chen, I. I. Pottosin, T. A. Cuin, A. T. Fuglsang, M. Tester, D. Jha, I. Zepeda-jazo, M. Zhou, M. G. Palmgren, I. A. Newman and S. Shabala, Root plasma membrane transporters controlling K^+/Na^+ homeostasis in salt-stressed barley, *Plant Physiol.*, 2007, **145**, 1714–1725.
68 L. Shabala, T. A. Cuin, I. A. Newman and S. Shabala, Salinity-induced ion flux patterns from the excised roots of *Arabidopsis* sos mutants, *Planta*, 2005, **222**, 1041–1050.
69 A. Sosan, D. Svistunenko, D. Straltsova, K. Tsiurkina, I. Smolich, T. Lawson, S. Subramaniam, V. Golovko, D. Anderson, A. Sokolik, I. Colbeck and V. Demidchik, Engineered silver nanoparticles are sensed at the plasma membrane and dramatically modify the physiology of *Arabidopsis* thaliana plants, *Plant J.*, 2016, **85**, 245–257.
70 J. K. Zhu, Abiotic stress signaling and responses in plants, *Cell*, 2016, **167**, 313–324.
71 T. A. Cuin and S. Shabala, Compatible solutes reduce ROS-induced potassium efflux in *Arabidopsis* roots, *Plant, Cell Environ.*, 2007, **30**, 875–885.
72 J. You and Z. Chan, ROS regulation during abiotic stress responses in crop plants, *Front. Plant Sci.*, 2015, **6**, 1092.
73 G. Adem, S. J. Roy, M. Zhou, J. P. Bowman and S. Shabala, Evaluating contribution of ionic, osmotic and oxidative stress components towards salinity tolerance in barley, *BMC Plant Biol.*, 2014, **14**, 113.
74 S. C. Fry, J. G. Miller and J. C. Dumville, A proposed role for copper ions in cell wall loosening, *Plant Soil*, 2002, **247**, 57–67.
75 S. C. Fry, Primary cell wall: tracking the careers of wall polymers in living plant cells, *New Phytol.*, 2004, **161**, 641–675.
76 J. Foreman, V. Demidchik, J. H. F. Bothwell, P. Mylona, H. Miedema, M. A. Torres, P. Linstead, S. Costa, C. Brownlee, J. D. G. Jones, J. M. Davies and L. Dolan, Reactive oxygen species produced by NADPH oxidase regulate plant cell growth, *Nature*, 2003, **422**, 442–446.
77 M. Jayakannan, J. Bose, O. Babourina, Z. Rengel and S. Shabala, Salicylic acid improves salinity tolerance in *Arabidopsis* by restoring membrane potential and preventing salt-induced K^+ loss via a GORK channel, *J. Exp. Bot.*, 2013, **64**, 2255–2268.
78 H. Wu, L. Shabala, M. Zhou and S. Shabala, Chloroplast-generated ROS dominate NaCl-induced K^+ efflux in wheat leaf mesophyll, *Plant Signaling Behav.*, 2015, **10**, e1013793.
79 J. Bose, L. Shabala, I. Pottosin, F. Zeng, A. Velarde-Buendie, A. Massart, C. Poschenrieder, Y. Hariadi and S. Shabala, Kinetics of xylem loading, membrane potential maintenance, and sensitivity of K^+-permeable channels to reactive oxygen species: physiological traits that differentiate salinity tolerance between pea and barley, *Plant, Cell Environ.*, 2014, **37**, 589–600.
80 X. Ma, L. Deng, J. Li, X. Zhou, N. Li, D. Zhang, Y. Lu, R. Wang, J. Sun, C. Lu, X. Zheng, E. Fritz, A. Hüttermann and S. Chen, Effect of NaCl on leaf H^+-ATPase and the relevance to salt tolerance in two contrasting poplar species, *Trees*, 2010, **24**, 597–607.
81 P. Silva and H. Gerós, Regulation by salt of vacuolar H^+-ATPase and H^+-pyrophosphatase activities and Na^+/H^+ exchange, *Plant Signaling Behav.*, 2009, **4**, 718–726.
82 E. Bassil, H. Tajima, Y. C. Liang, M. A. Ohto, K. Ushijima, R. Nakano, T. Esumi, A. Coku, M. Belmonte and E. Blumwald, The *Arabidopsis* Na^+/H^+ antiporters NHX1 and NHX2 control vacuolar pH and K^+ homeostasis to regulate growth, flower development, and reproduction, *Plant Cell*, 2011, **23**, 3482–3497.
83 A. M. Ismail and T. Horie, Genomics, physiology, and molecular breeding approaches for improving salt tolerance, *Annu. Rev. Plant Biol.*, 2017, **68**, 405–434.
84 S. L. Richards, K. A. Wilkins, S. M. Swarbreck, A. A. Anderson, N. Habib, A. G. Smith, M. McAinsh and J. M. Davies, The hydroxyl radical in plants: from seed to seed, *J. Exp. Bot.*, 2015, **66**, 37–46.
85 P. Schopfer, Hydroxyl radical-induced cell-wall loosening *in vitro* and *in vivo*: Implications for the control of elongation growth, *Plant J.*, 2001, **28**, 679–688.
86 K. Muller, A. Linkies, R. A. M. Vreeburg, S. C. Fry, A. Krieger-Liszkay and G. Leubner-Metzger, *In vivo* cell wall loosening by hydroxyl radicals during cress seed germination and elongation growth, *Plant Physiol.*, 2009, **150**, 1855–1865.
87 L. H. Hao, W. X. Wang, C. Chen, Y. F. Wang, T. Liu, X. Li and Z. L. Shang, Extracellular ATP promotes stomatal opening of *Arabidopsis thaliana* through heterotrimeric G protein α subunit and reactive oxygen species, *Mol. Plant*, 2012, **5**, 852–864.
88 S. Signorelli, E. L. Coitiño, O. Borsani and J. Monza, Molecular mechanisms for the reaction between $^{\cdot}OH$ radicals and proline: Insights on the role as reactive oxygen species scavenger in plant stress, *J. Phys. Chem. B*, 2014, **118**, 37–47.
89 A. Yadav and P. C. Mishra, Modeling the activity of glutathione as a hydroxyl radical scavenger considering its neutral non-zwitterionic form, *J. Mol. Model.*, 2013, **19**, 767–777.
90 J. Treml and K. Smejkal, Flavonoids as potent scavengers of hydroxyl radicals, *Compr. Rev. Food Sci. Food Saf.*, 2016, **15**, 720–738.
91 M. K. van Ittersum, L. G. J. van Bussel, J. Wolf, P. Grassini, J. van Wart, N. Guilpart, L. Claessens, H. de Groot, K. Wiebe, D. Mason-D'Croz, H. Yang, H. Boogaard, P. A. J. van Oort, M. P. van Loon, K. Saito, O. Adimo, S. Adjei-Nsiah, A. Agali, A. Bala, R. Chikowo, K. Kaizzi, M. Kouressy, J. H. J. R. Makoi, K. Ouattara, K. Tesfaye and K. G. Cassman, Can sub-Saharan Africa feed itself?, *Proc. Natl. Acad. Sci. U. S. A.*, 2016, **113**, 14964–14969.
92 P. Rengasamy, World salinization with emphasis on Australia, *J. Exp. Bot.*, 2006, **57**, 1017–1023.
93 S. Dasgupta, M. M. Hossain, M. Huq and D. Wheeler, Climate change and soil salinity: The case of coastal Bangladesh, *Ambio*, 2015, **44**, 815–826.

94 J. Han, J. Shi, L. Zeng, J. Xu and L. Wu, Effects of nitrogen fertilization on the acidity and salinity of greenhouse soils, *Environ. Sci. Pollut. Res.*, 2015, **22**, 2976–2986.

95 M. Qadir, E. Quillérou, V. Nangia, G. Murtaza, M. Singh, R. J. Thomas, P. Drechsel and A. D. Noble, Economics of salt-induced land degradation and restoration, *Nat. Resour. Forum*, 2014, **38**, 282–295.